IEEE Robotics and Automation Letters (RA-L) paper, presented at ICRA 2024, Yokohama, Japan. Cite as RA-L paper.

Control and Implementation of a Fluidic Elastomer Actuator for Active Suppression of Hand Tremor

Yixin Wang[1], Xin-Jun Liu[1], and Huichan Zhao[1]

***Abstract*—Active exoskeletons for tremor suppression show potential for treatment of pathological tremor thanks to their non-invasive nature. However, the active force was only used for the voluntary movement following. As a potential alternative, fluidic elastomer actuators (FEAs) possess compliance and flexibility that is important for wearable devices. In this study, we introduce the control implementation for a FEA to the application of active suppression of hand tremor, which allows a wearable FEA actively exerting force on the finger against tremor and meanwhile following the voluntary motion. The proposed pressure control algorithm could push the closed-loop pressure control to 19 Hz cutoff frequency. A combination neural network of GRU-MLP (Gated Recurrent Unit-Multilayer Perceptron) was proposed to identify and control a fiber-reinforced FEA following the voluntary movement of hand. The active tremor suppression effectiveness of the proposed method was tested on a bench-top tremor simulator, and such method could suppress the hand tremor from the original amplitude of more than 5° to less than 1°. The proposed method paves a new way for tremor suppression exoskeletons.**

***Index Terms*—Modeling, control and Learning for soft robotics, neural and fuzzy control, prosthetics and exoskeletons.**

I. Introduction

APROXIMATELY 60% of those people affected by pathological tremor (PT) experience movement disability in their activities of daily living because of the involuntary, rhythmic oscillations of body parts[1], [2]. Amid the treatments for PT, exoskeletons for tremor suppression have shown advantages and application potentials due to their relatively low cost and the non invasive nature[3], [4]. Recent studies in this field are classified into three major strategies: active methods that apply active force on the human body[5], [6], [7], [8], passive methods that utilize mechanical dampers with a fixed value of damping[9], and semi-active methods utilizing mechanical dampers with an adjustable value of damping [10]. Active methods possess superiority such as their full suppression of tremors due to their abilities to exert active force on the body against tremors. However, these active methods did not exert active force on finger for resisting against tremor and instead only utilized the active force to follow the voluntary movement and relied on the passive resistance of exoskeletons to achieve tremor suppression.

Soft exoskeletons driven by fluidic elastomer actuators (FEAs) have the characteristics of comfort and safety due to the inherent compliance of the materials they are constructed from [11], [12], [13], using gas instead of liquid in the system adds an additional layer of compliance to the exoskeletons. Relevant studies have shown that there is a mapping relationship between the internal pressure and the output force of FEAs [14], [15], thus making it feasible to exert active force by rapidly regulating the internal pressure. For active suppression of hand tremor, nevertheless, FEAs still lack the following two subsystems: i) A pressure supply system (PSS) to provide sufficient speed of response for generating fast-changing pressure, and ii) algorithms that enable the FEAs to identify and follow voluntary movements in the mixed signals of tremor movements while exerting active force on the finger against the tremor.

For the PSS, our previous work established a comprehensive pressure and flow dynamic model of high speed PSSs and demonstrated that for a cylinder-driven PSS, the pressure could follow the movement of the piston at a frequency as high as 39 Hz with negligible delay in phase and attenuation in amplitude [16]. At such a frequency, it is feasible to generate pressure that powers an FEA to suppress PT, as the frequency of PT is commonly in a range of 3 Hz to 10 Hz[17], [18]. However, such a PSS still lacks a closed-loop pressure control method with sufficient response speed. For the identification of voluntary movement from tremor, low-pass and high-pass digital filters were used [6], [7], but they had inherent problems of time lag, meaning a certain time delay between the identified voluntary movement and that of the ground truth. Ibrahim et al. used a neural network for the first time to identify voluntary movement [19], in which they utilized a combination of one dimensional convolution neural network (1D-CNN) and multilayer perceptron (MLP) in the computing of the time series of the mixed movement and finally generated the identified signal of voluntary movement. Results showed that such a neural network could identify voluntary movement with sufficient precision and without the problem of time lag.

In this study, we introduce a complete control system for a fiber-reinforced FEA for the active suppression of hand tremor, which is implemented on a wearable FEA-based device (Fig. 1a). Compared with the previous active tremor suppression strategies, we control a FEA to actively exert force

Manuscript received: July, 21, 2023; Revised October, 17, 2023; Accepted November, 25, 2023.

This paper was recommended for publication by Editor Pietro Valdastri upon evaluation of the Associate Editor and Reviewers' comments. This work was supported by the National Natural Science Foundation of China under Grant Nos. 52222502, 51975306, and 92048302. (*Corresponding author: Yixin Wang)*

[1]Yixin Wang, Xin-Jun Liu and Huichan Zhao are with the Department of Mechanical Engineering, State Key Laboratory of Tribology in Advanced Equipment, Beijing Key Lab of Precision/Ultra-Precision Manufacturing Equipment and Control, Tsinghua University, China wang-yx1993@foxmail.com; xinjunliu@mail.tsinghua.edu.cn; zhaohuichan@mail.tsinghua.edu.cn

Digital Object Identifier (DOI): see top of this page.

IEEE Robotics and Automation Letters (RA-L) paper, presented at ICRA 2024, Yokohama, Japan. Cite as RA-L paper.

IEEE Robotics and Automation Letters (RA-L) paper, presented at ICRA 2024, Yokohama, Japan. Cite as RA-L paper.

TABLE I
COMPARISON OF ACTIVE TREMOR SUPPRESSION STRATEGIES

Author	Actuator	Usage of active force
Zhou [5]	Brushless motor	Tracking voluntary movement
Herrnstadt [7]	Brushless motor	Tracking voluntary movement
Skaramagkas [8]	FEA	Applying constant force on fingertip
This work	FEA	Tracking voluntary movement and suppressing tremor movement

on a finger to resist against tremor and meanwhile allow the tracking of the voluntary movement (Table I).

We first propose and implement a feedforward control algorithm to generate any pressure from a cylinder-driven PSS based on the adiabatic process of the gas in the cylinder. In the subsequent experiments, such a PSS is used as a pressure servo. We then proposed a pressure prediction model based on MLP which can predict the inner pressure of a fiber-reinforced FEA according to the voluntary movement signal. Subsequently, in the task of tremor signal separation, we propose a tremor identification model based on a gated recurrent unit (GRU) and compare the prediction results with a conventional digital filter. Furthermore, based on the integration of aforementioned algorithms and models, an adaptive tremor suppression algorithm is proposed and implemented, which allows the FEA to actively exert force to suppress the tremor, and the effect of suppression is validated on a simulated finger with PT.

The main contributions of this study are as follows:

1) A feedforward pressure control algorithm used in cylinder-driven PSS that can push the response speed of pressure to the speed limit of the cylinder piston.
2) A control method that integrates two neural networks of MLP and GRU, allowing the precise and synchronous following of the FEA movement to the voluntary movement in the mixed movement of tremor.
3) An adaptive and active tremor suppression algorithm, allowing the FEA to exert active force against tremor to achieve an improved suppression effect.

II. METHODS

A. Tremor-suppressing FEA design and experimental setups

We designed a fiber-reinforced FEA to suppress the tremor on the human finger. As showed in Fig. 1b, the structure of the FEA is basically a hollow silica rubber wrapped with a series of nylon fiber hoops. When inflated the elastomer will deform only along the long axis due to the limitation of the outer hoop-shaped nylon reinforce layer. As is shown in Fig. 1a, in its worn state, one end of the FEA is fixed on the base (e.g., the palm) and the other end is fixed on the finger (e.g. the proximal phalange). In such a state, the FEA bends upon inflation and can exert a bending torque to the joint it includes.

We established a bench-top device to test our control on FEA. As showed in Fig. 1a, the device was a shaft driven by a servo motor (Key Fulcrum K7361V2, Himark Aero Tech Co., Ltd., Zhuhai, China). A 3D-printed finger was directly fixed to a rectangular shaft and its bending movement around the axis of shaft is transmitted to an encoder (ENC-4096, PUDI Electronic Co., Ltd., Dongguan, China) through a coupling. The readings of the encoder were regarded as actual bending movement signal of the finger. The finger was driven by the servo motor through a 3D-printed torsional spring to simulate the original movement of finger. We regulated the stiffness of the spring to a value of 0.13 N m/rad by adjusting its geometrical parameters such as thickness of the spring plate and number of the spring plate, which similar to human finger joint (0.09 N m/rad) [20].

With the connection of the servo motor, the device showed in Fig. 1a was used for the experiments that verify the voluntary movement identification and the tremor suppression abilities of the proposed algorithms. Without the connection of the servo motor, the device was used for the data collection experiments and validation experiments of the MLP model. The disconnection of the servo motor from the spring was to realize a condition that the bending of the finger is only driven by the FEA.

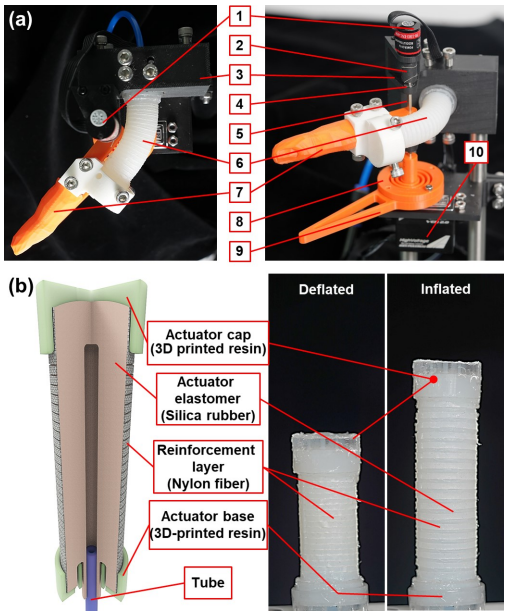

Fig. 1. Tremor-suppressing FEA design and experimental setup with a simulated finger. (a) Simulated finger setup for evaluating the tremor suppression and voluntary movement following of the wearable FEA. The setup consists of an encoder-1, a coupling-2, a base-3, a pair of bearings-4, a rectangular shaft-5, a fiber-reinforced FEA-6, a 3D-printed finger-7, a 3D printed torsional spring-8, a 3D-printed indicating plate of the motor's motion-9 and a servo motor-10. (b) Structural diagram of the fiber-reinforced FEA.

Fig. 2a depicts another setup that we used to evaluate the FEA's capability of following the voluntary movement of the finger. This setup was similar to the one in Fig. 1a, instead of using a motor, there was a handle that could be moved manually to exert an arbitrary force to the simulated finger through a force transducer (Nano17 Titanium, ATI Industrial Automation, Inc., North Carolina, USA). The handle was mounted on the shaft by a pair of bearings to ensure the driving force will be completely applied on the finger through the force transducer. The transducer between the handle and

IEEE Robotics and Automation Letters (RA-L) paper, presented at ICRA 2024, Yokohama, Japan. Cite as RA-L paper.

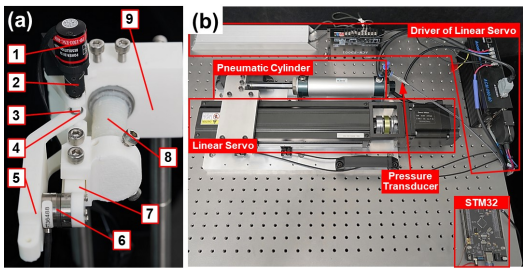

Fig. 2. Experimental setups. (a) Experimental setup for evaluating the resistance that FEA applies to the finger during the voluntary movement following control. The setup consists of an encoder-1, a coupling-2, a shaft-3, a pair of bearings-4, a handle-5, a force transducer 6, a 3D printed finger-7, a fiber-reinforced FEA 8, and a base-9. (b) Experimental setup of the pressure servo.

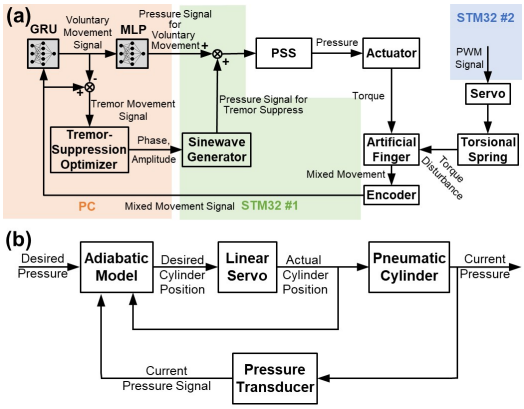

Fig. 3. Control block diagrams. (a) The whole tremor suppression system. (b) The detailed control block diagram of the PSS in (a).

the finger was to record the resistance force of the FEA to the finger, and the value of the force was conversed to torque by multiplication of the distance between the transducer to the shaft. This device was used to compare the resistance of different voluntary movement identification algorithms.

Fig. 2b shows the setup of the PSS driven by a cylinder (MAL40×100, Wenzhou Jiangxin pneumatic hydraulic Co., Ltd., Zhejiang, China). A linear servo motor (ACM 090 60, Copley Controls Co., Canton, USA) drove the piston of the cylinder to generate changing pressure in the cylinder. The pressure was recorded by a pressure transducer (SCYG314, WUXI SEN measurement control technology Co., Ltd., Jiangsu, China) installed at the outlet of cylinder. The desired position signal and the actual position signal of the linear servo were transmitted between its driver and the MCU (#1) (STM32F407VE, STMicroelectronics International NV., Geneva, Switzerland) via CANopen bus.

B. Overview of Control System

Fig. 3a shows the complete block diagram of the active tremor suppression system, in which the experimental setup corresponds to that shown in Fig. 1a. A PWM signal generated by a separate MCU (#2) (STM32F407VE, STMicroelectronics International NV., Geneva, Switzerland) drove the servo to generate a mixed movement of voluntary and tremor, which was transmitted to the simulated finger as a torque disturbance through the torsional spring. The mixed movement of the finger was collected by the encoder and fed to the GRU model to predict the low-frequency voluntary movement. Subsequently, the predicted voluntary movement was fed to the MLP model to predict the pressure's low frequency component, which enabled the FEA to follow the voluntary movement of the finger. Simultaneously, the tremor movement signal was obtained based on the difference between the predicted voluntary movement and the mixed movement and fed to the tremor-suppression optimizer, which could give the optimized amplitude and phase of the oscillating component of the pressure driving signal, which was for actuating the FEA to generate the active force against the tremor. The aforementioned two components of pressure were fused and fed to the PSS, and the actual pressure was propagated to FEA through a tube to achieve the goal of following voluntary movement and meanwhile suppressing tremor movement of the finger.

In order to speed up the control loop, we used a personal computer (CPU: Inter Core i7-7700HQ, 2.8 GHz; GPU: NVIDIA GeForce 940MX, 8GB; RAM: 16GB) to execute the training of GRU and MLP models and the tremor suppression optimizer, and an MCU (#1) to execute the fusion of pressure signals, the pressure control, the collection of encoder signals, and the generation of sinusoidal pressure signals for active suppressing of the tremor. The computer and MCU (#1) communicated through a serial port, and the update frequency of the control loop was 100 Hz.

C. Pressure Control Algorithm

Fig. 3b shows the detailed control block diagram of the PSS block in Fig. 3a, where the experimental setup corresponds to Fig. 2b. The adiabatic model in the diagram is the adiabatic process of the air inside the cylinder:

$$\frac{p_n}{\rho_n^\kappa} = \frac{p_{n-1}}{\rho_{n-1}^\kappa} \tag{1}$$

where p is the gas pressure in cylinder, ρ is the density of the gas in cylinder, κ is the specific heat ratio of gas, and the subscript n and $n-1$ stand for the n–th and $(n-1)$–th control cycle, respectively. Replacing the density with a quotient of mass and volume and deleting the mass terms on both sides could give:

$$p_n L_n^\kappa = p_{n-1} L_{n-1}^\kappa \tag{2}$$

where L is the relative position of the piston inside the cylinder. Rearranging (2) could give:

$$L_n = L_{n-1} \left(\frac{p_{n-1}}{p_n} \right)^{\frac{1}{\kappa}} \tag{3}$$

From (3), we could calculate the desired piston position based on the piston position and pressure of the previous control cycle (which could be measured) and the current desired pressure. The calculated desired piston position was sent to the driver of linear servo motor for execution. The above procedures could realize the feedforward closed loop control of the pressure in the cylinder.

IEEE Robotics and Automation Letters (RA-L) paper, presented at ICRA 2024, Yokohama, Japan. Cite as RA-L paper.

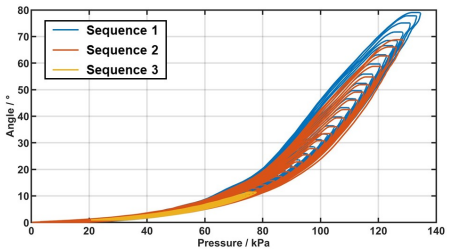

Fig. 4. Training set of the MLP model that is used to predict the internal pressure of the FEA based on desired voluntary bending angle of the finger.

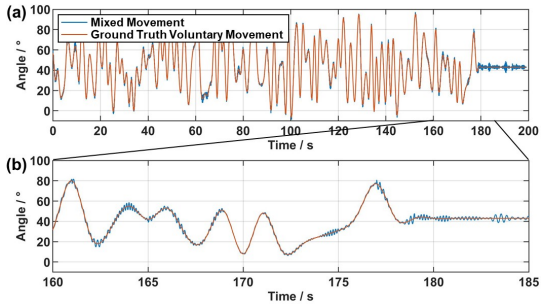

Fig. 5. Training set of the GRU model used to separate voluntary movement signal from mixed movement signal of voluntary and tremor movement. (a) Overview of the training set. (b) Partial enlarged details in the time range from 165 s to 185 s

In practice, there are two factors affecting the justification of adiabatic assumption: heat exchange between the gas in cylinder and the environment, as well as gas flow between the cylinder and FEA. To address these deviations, as shown in Fig. 3b, we fed the pressure of the gas in the cylinder and the position of the cylinder piston back at a frequency of 400 Hz in the control loop, making (3) based only on the process of gas in cylinder as ideal adiabatic process in a time scale of 2.5 ms. The pressure change caused by the aforementioned two factors becomes negligible under such short time scale, thus ensuring rationality and accuracy of the adiabatic assumption used in (3).

D. MLP Model

We used an MLP model with 4 hidden layers, 128 neurons in each layer, and an activation function of tanh in each neuron, to predict the driving pressure of FEA based on desired bending angle. Such a structure provides a good balance between computational speed and prediction accuracy. Considering that recent studies using neural networks to control FEA involved the information of historical control status[15], the input of MLP in this study was set to be the voluntary movement signal that predicted by the GRU model for the last 8 control cycles. The model was supposed to predict the driving pressure for the FEA to reach the desired bending angle in real time, through the training of quite an amount of collected experimental data with bending angles and pressures of the FEA. We used the aforementioned PSS to generate changing pressures to drive the FEA bending to different positions, during which we collected the information of bending angles and pressures with the experimental setup shown in Fig. 1a (the servo motor was disconnected from the torsional spring to realize a condition that the 3D-printed finger and FEA are completely free from external disturbances, where the bending of finger was only driven by the FEA.) at a sampling rate of 100 Hz. The collected data were then used to train the MLP model. To capture the relationship between the FEA bending angles and the driving pressures as comprehensive as possible thus the model can predict the pressure more accurately, we designed three 50-second damping oscillation pressure sequences with different amplitudes and different equilibrium positions for the training set, and the collected data are shown in Fig. 4.

E. GRU Model

The GRU model, frequently employed in time sequence processing, was introduced by Cho et al. [21] to address the challenges of long-term memory and unstable gradient in recurrent neural networks (RNNs). A single GRU cell shares the same interfaces as an RNN cell, including input, previous hidden state, output, and current hidden state. This cell computes the output and current hidden state based on input and previous hidden state for each new data point in a time sequence. Such processing enables the hidden state to retain crucial information during time series input. The concept of GRU relies on the regulating of the information in hidden state by two gated units inside the GRU cell: reset gate and upgrade gate. The reset gate determines how much information from the previous hidden state should be forgotten, while the update gate decides how much information from the current input should be stored in the hidden state. These gates allow for continuous updating of the hidden state when new data points of time series are fed into network to recognize and remember specific patterns during processing. Consequently, such networks possess capabilities for isolating or predicting specific information within a time series.

In this study, a GRU with 2 hidden layers, 20 neurons in each layer, and an activation function of tanh in each neuron was used to separate the voluntary movement signal from the mixed signal of voluntary and tremulous movement. The input of the model was the original signal recorded in the last 100 control cycles, and the output was the signal of the separated voluntary movement.

Since the frequency of human voluntary movement is mainly within 1 Hz whereas that of pathological tremor is mainly within the range of 3 Hz to 10 Hz [17], [18], we used randomly generated sequences of different frequencies mixed together as the training set of GRU. The voluntary movement was obtained by the spline interpolation of a random number sequence in a range of 0° to 90°, in which the time interval of interpolation was 0.01 s, and that of the random number sequence was 1 s. The tremor movement was a series of periodic signals with a time interval of 0.01 s, an amplitude in the range of 0° to 5°, and a frequency in the range of 3 Hz to 10 Hz.

Using the above method, a mixed movement signal with

IEEE Robotics and Automation Letters (RA-L) paper, presented at ICRA 2024, Yokohama, Japan. Cite as RA-L paper.

IEEE Robotics and Automation Letters (RA-L) paper, presented at ICRA 2024, Yokohama, Japan. Cite as RA-L paper.

a total duration of 200 s was generated for training the GRU model, as shown in Fig. 5a. To enable the model to recognize both moving and stationary voluntary movements, a stationary voluntary movement was inserted between 180 s and 200 s in the training set, as shown in Fig. 5b.

The two neural models (MLP and GRU) were trained and deployed using Python 3.7 and TensorFlow 2.3, with an optimizer of Adam and iterations of 300. The trained GRU model was converted to the format of .tflite in order to increase the computational speed.

F. Adaptive Tremor Suppression Optimizer

In order to make the FEA actively output the torque for tremor suppressing, an adaptive optimizing algorithm based on the minimum mean square of tremor signal is proposed. In the algorithm, a sinusoidal form of pressure signal was adopted and its phase and amplitude were regulated based on the tremor signals adaptively.

Once the tremor suppression is enabled, the optimizer in Fig. 3a firstly treats the tremor signal within the last 1 s as an ideal sinusoidal signal and identifies its phase based on the time stamp of the peaks. Assume the tremor signal is a sinusoidal signal with amplitude A, frequency f, and phase ϕ, and then the phase could be described as follows:

$$2\pi f t_p^i + \phi^i = \frac{pi}{2} \tag{4}$$

where t_p^i is time stamp corresponding to the i–th peak of the tremor signal, ϕ_i is the phase of the signal that is calculated according to the i–th peak. The following equation is used to normalize the phase to a range of -π–π:

$$\hat{\phi}^i = \phi^i - 2\pi \cdot round\left(\frac{\phi^i}{2\pi}\right) \tag{5}$$

where $round\,(\cdot)$ is the rounding algorithm. The phase that calculated by all peaks within 1 s are averaged to get final phase of tremor signal to get more accurate identified phase:

$$\overline{\phi} = \frac{\sum_{i=1}^{n} \hat{\phi}^i}{n} \tag{6}$$

As the pressure signal used for tremor suppression needs to be in a phase opposite to the tremor action, that is, there is a phase difference of π radians between the actual pressure signal and tremor signal, therefore, the phase that transmitted from the optimizer to the sine wave generator could be expressed as:

$$\phi_s = \overline{\phi} + \pi + \phi_{correct} \tag{7}$$

where $\phi_{correct}$ is the compensation value of the phase difference between actual and desired pressure value in PSS, which could be calculated according to the following formula:

$$\phi_{correct} = af + b \tag{8}$$

in which the value of parameter a and b were obtained by fitting the experimental phase-frequency characteristic curve of the actual pressure and desired pressure in PSS (the curve will be shown in later sections).

With a fixed value of $\phi_{correct}$, we used the gradient descent algorithm as the optimizer to regulate the amplitude of pressure signal that is supposed to suppress tremor, at an updating rate of 1 Hz. The optimization direction is set to be the negative gradient of the $Cost$:

$$A_s^n = A_s^{n-1} - \mu\frac{\partial Cost}{\partial A_s} = A_s^{n-1} - \mu\frac{Cost^{n-2} - Cost^{n-1}}{A_s^{n-2} - A_s^{n-1}} \tag{9}$$

where A_s is the amplitude of the pressure signal, and superscript n stand for the n–th update step. μ is the adjustment step with value of 0.005 (kPa/°)^2, and $Cost$ is the mean square value of the movement signal of tremor recorded in last 1 s. In the first two update step, the value of A_s^1 and A_s^2 is intuitively set to 3 kPa to 3.5 kPa, respectively. Therefore, the initial gradient of $Cost$ could be calculated based on $Cost^1$ and $Cost^2$ through first order difference and start the iteration described by (9) from third update step.

III. Results and Discussion

A. Frequency Response of PSS

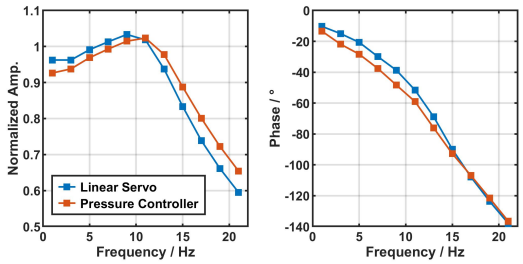

Fig. 6. Frequency response curves of PSS. (a) Normalized amplitude frequency curves. (b) Phase frequency curves.

Fig. 6 shows the frequency response curve of the PSS obtained by experiment, during which the host MCU (#1) was used to generate the sinusoidal signals with different frequencies, and the amplitude and phase difference between the actual signal and the reference signal were recorded and analyzed. The blue lines in Fig. 6 represent the frequency response of the actual position of the linear servo relative to the desired position, and the orange lines represent the frequency response of the actual pressure of PSS relative to the desired pressure. It can be seen from Fig. 6 that for the amplitude-frequency response of the pressure control in PSS, its cut off frequency reaches approximately 19 Hz, which is sufficient to generate the pressure signal required to suppress tremor (usually 3 Hz to 10 Hz[17], [18]). In addition, the frequency response curves of the position loop in the linear servo basically coincide with those of the pressure loop, indicating that the pressure control algorithm proposed in this paper has pushed the dynamic performance of the pressure generation to its upper limit.

B. Voluntary Movement Following using MLP

In the control system, the host MCU (#1) was used to generate signals of different frequencies, which were then sent to the MLP model to predict the pressure in FEA, and such

IEEE Robotics and Automation Letters (RA-L) paper, presented at ICRA 2024, Yokohama, Japan. Cite as RA-L paper.

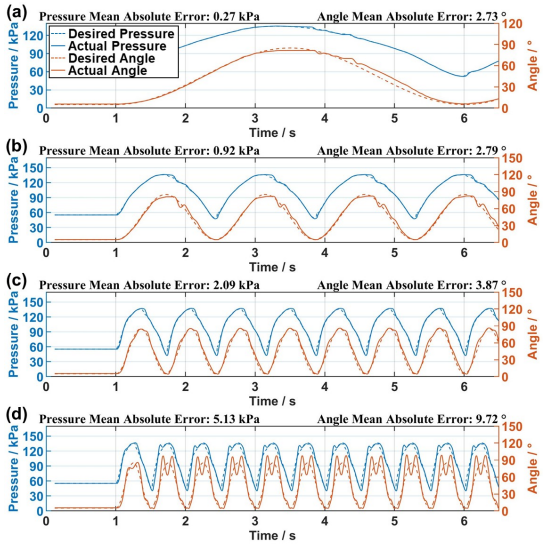

Fig. 7. Pressure and bending angle signals collected in the control experiment of PSS and MLP model with voluntary movement signal have frequency of (a) 0.2 Hz, (b) 0.8 Hz, (c) 1.4 Hz, (d) 2.0 Hz.

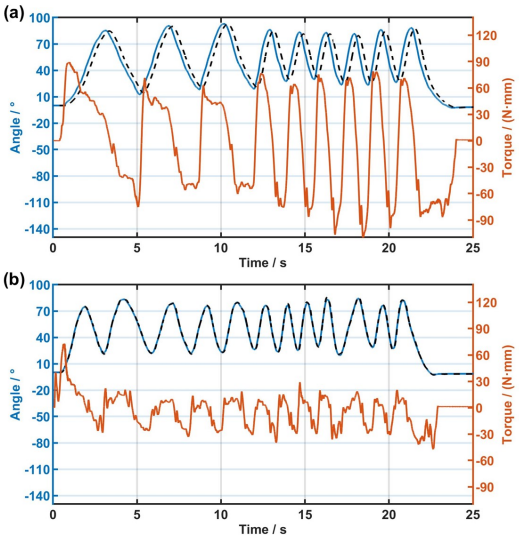

Fig. 8. Moving experimental result to verify the voluntary movement following ability with (a) 4th ordered Butterworth filter and (b) proposed GRU model as voluntary movement identification algorithm, respectively. The black dashed line in each subfigure represents the real-time voluntary movement filtered by corresponding algorithm.

signal was fed to the PSS to realize and finally drive the finger. Fig. 7 shows the signals of pressure and finger movement when FEA follows the voluntary movement signals of different frequencies of 0.2 Hz to 2.0 Hz base on the pressure predicted by MLP model. The mean absolute error (MAE) between the desired and actual pressure in PSS is in a range of 0.27 kPa to 2.09 kPa (Relative error: 0.36%-2.8%) when frequency of voluntary movement is no more than 1.4 Hz, indicating that PSS is able to accurately follow the dynamic pressure signals. Besides, the MAEs of the MLP controlled FEA following the voluntary movement signals of multiple frequencies are in the range of 2.6° to 3.9° (relative error: 2.8% to 4.1%), indicating its accuracy in following voluntary movements up to 1.4 Hz. When the frequency increased by 2 Hz, the inertia of the actuator and finger caused the finger vibrate at a bending angle around 85°, which was regarded as the upper limit of the frequency of voluntary movement that can be followed.

C. Voluntary movement identification with GRU

The experiment in this section was achieved by moving the handle manually in Fig. 2a and collecting the signals of both encoder and force transducer synchronously. The movement of 3D printed finger was captured by the encoder and fed to the GRU model, the output signals of GRU was regarded as that of voluntary movement and fed to the MLP model, generating the pressure signal to drive the FEA to bend and follow the handle. Ideally, the force transducer would always record zero forces as the FEA was dynamically pushing the handle to follow the movement.

Fig. 8a and b show the finger rotation angle and the resistive torque (recorded by the readings of the force transducer times the arm length) when a 4th-ordered Butterworth filter with a cutoff frequency of 1 Hz and the GRU are used to identify the voluntary movement signal, respectively (see Supplementary Video Section 1. Moving Experiment). With the Butterworth filter, the MAE of the moving resistance torque is 49.59 N mm, while that with GRU is 15.05 N mm, which is significantly reduced using GRU. Such an effect indicates a much smaller resistance caused by the exoskeleton when following voluntary movement and an increased comfort as wearable devices.

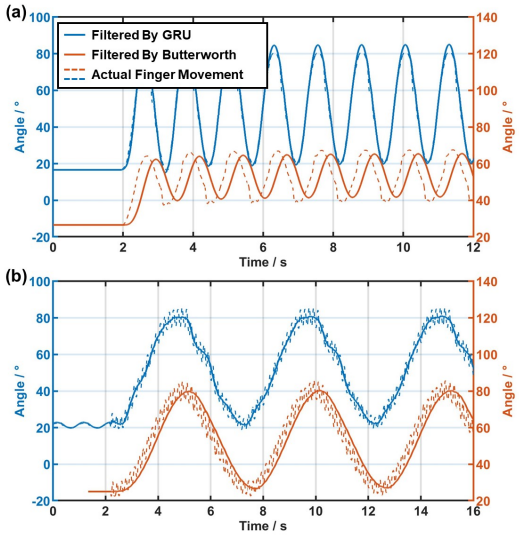

Fig. 9. Voluntary movement identifying and following ability with GRU and MLP. (a) 0.8 Hz voluntary movement of 20° to 80° without tremor. (b) 0.2 Hz voluntary movement of 20° to 80° with a 6 Hz tremor.

The abilities of the whole system following the voluntary movement with and without tremor disturbance were verified utilizing experiment setup shown in Fig. 1a and the control system shown in Fig. 3a, in which the servo motor was connected to the torsional spring and the active suppression was disabled in the system. We compared the effect of the control algorithm using the Butterworth filter and GRU on the

IEEE Robotics and Automation Letters (RA-L) paper, presented at ICRA 2024, Yokohama, Japan. Cite as RA-L paper.

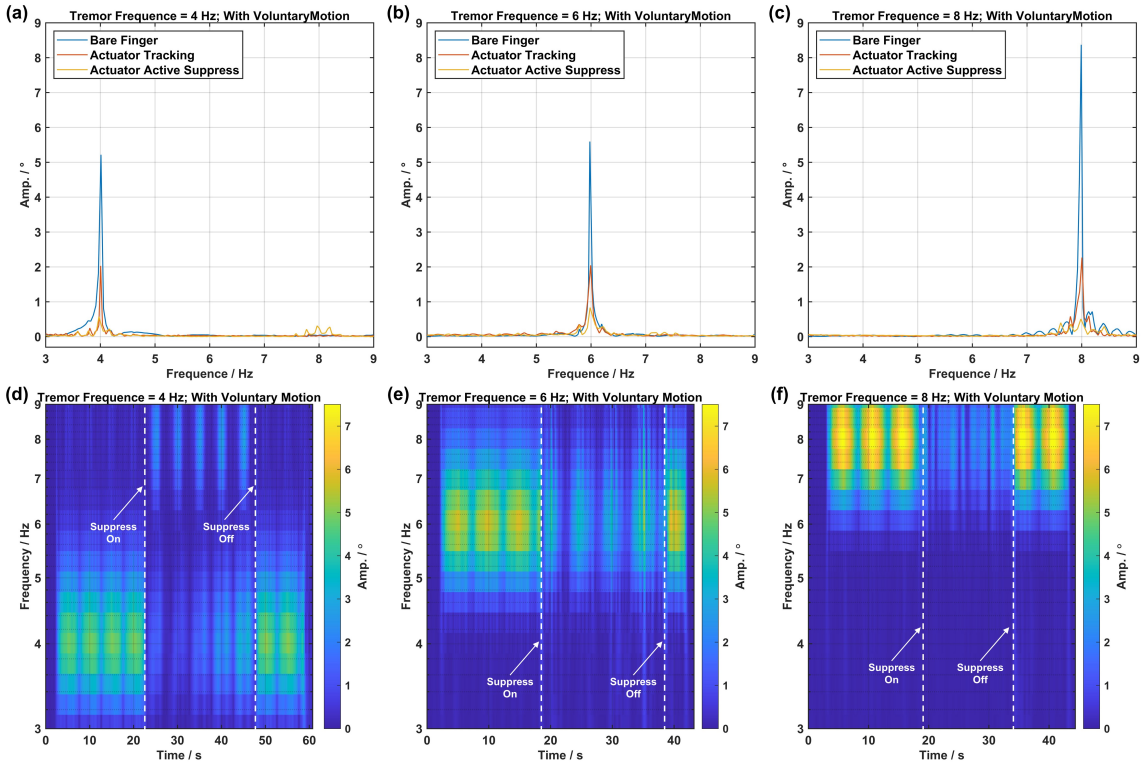

Fig. 10. Visualization of spectrums of original and suppressed tremor by FEA. (a)–(c) Amplitude spectrums of tremor movement with bare finger, suppressed by voluntary movement following and suppressed by active suppress algorithm, respectively. (d)–(f) Time-frequency spectrums of the finger movement that is recorded when the active tremor suppression is continuously turned on and off.

voluntary movement following of the FEA. The servo motor provided the same sinusoidal voluntary movements in a range of 20° to 80° at a frequency of 0.8 Hz. Results in Fig. 9a shows that the algorithm using the Butterworth filter yields a tracking movement in a range of 28° to 60° and with time lag of 290 ms, whereas the GRU yields a tracking movement in a range of 20° to 80°, with negligible time lag. Both the comparisons of time lag of the identified movement in Fig. 8 and Fig. 9 indicate it is the time lag of the Butterworth filter in identifying voluntary movement that causes non-trivial resistance from FEA to the finger, thereby reducing the amplitude of the actual followed voluntary movement.

The tremor disturbance with voluntary movement was provided by the mixed movement of servo motor that contains a sinusoidal movement of 0.2 Hz in the range of 20° to 80° as voluntary and a sinusoidal movement of 6 Hz with the amplitude of 5° as tremor. Results in Fig. 9b shows that both the GRU and the Butterworth filter could identify the voluntary movement and control the FEA to follow the voluntary movement with the presence of tremor disturbance. Both followed voluntary movements of FEA controlled by the GRU and the Butterworth filter are basically consistent with the reference movement from the servo motor. This consistency is because the time lag caused by the Butterworth filter is not significant compared the low frequency (0.2 Hz in this experiment) of the voluntary movement, which reduces the resistance of the FEA following the voluntary movement, and therefore has less influence on the voluntary movement.

Compared with the digital filter algorithm such as the Butterworth filter, the GRU model could ensure both accuracy and zero-time lag of identifying voluntary movement under disturbance of tremor at a higher frequency, so that the system exhibit a lower interference with the voluntary movement from the wearable FEA, demonstrating the potential of GRU as a good alternative for identifying voluntary movement in the mixed movement of both voluntary and tremor movement.

D. Active Tremor Suppression

In order to verify the active tremor suppression algorithm proposed in this paper, the experimental setup showed in Fig. 1a and control system showed in Fig. 2a were used to test the algorithm. We recorded the movement signals under the same set and in three states: bare finger, finger with the FEA following voluntary movement only and finger with the FEA active tremor suppression enabled. According to the tremor movement reproduced on benchtop device in relative studies[5], [6], [22], the servo was set as a mixture of a sinusoidal movement of 0.2 Hz in the range of 20° to 80° as the voluntary movement and a sinusoidal movement with the amplitude of 5° and of three independent frequency of 4 Hz, 6 Hz and 8 Hz as the tremor. Based on the same aforementioned disturbance, the amplitude spectrums of the finger movement under the three states are shown in Fig. 10a–c. It can be seen that with different tremor frequencies, the tremor amplitude can be reduced by more than half only by the following of voluntary movement of FEA. This is mainly due the increased stiffness caused by the FEA's elasticity suppressing the tremor movement to a certain extent.

Fig. 10d–f shows the time-frequency spectrum of the finger movement recorded when the active tremor suppression function of FEA is continuously turn on and off under tremor disturbance of different frequencies. The time-frequency spectrum was obtained through the wavelet transformation of the recorded movement signal of finger. The results show that the active suppression force applied on the basis of FEA voluntary movement following can further suppress the tremor movement. After the active suppression algorithm was enabled, the optimizer could accurately identify the phase of tremor signal and generate the suppression pressure to immediately suppress tremor, and adaptively adjust the suppression pressure amplitude through the subsequent algorithm. The tremor amplitude of different frequencies was suppressed to smaller than 1°, demonstrating an improved effect on tremor suppression compared with the pure voluntary movement following. Section 2 in Supplementary Video shows the comparative demonstration of the above process.

IV. Conclusion

In this work we demonstrated the control and implementation of a wearable FEA that could actively suppress the hand tremor and simultaneously following the voluntary movement. The proposed system utilized the compliance and flexibility of FEA-based exoskeleton as well as the high efficiency of active tremor suppression method, paving a new way for tremor-suppression exoskeletons. The proposed control algorithms and system were tested and characterized on a platform that simulated both voluntary and tremor movement of finger. The proposed feedforward pressure algorithm increased the closed-loop cutoff frequency for pressure control of the cylinder-driven PSS to its upper limit. In particular, in the case of PSS with linear servo that has sufficient response speed, the pressure response speed of which could meet the requirements of tremor suppression. Compared with digital filtering algorithms used in related external tremor suppression devices to identify voluntary movement of the human body, the proposed combination networks of GRU and MLP possess less resistance in controlling the FEA to follow the voluntary movements of the finger, which is important for the user experience with wearable devices. Specifically, the ability of FEA to passively suppress finger tremor by its own elasticity when following the voluntary movement was found. The experimental data further shows that the proposed active tremor suppression algorithm could suppress the tremor amplitude to less than 1°. The control method and related algorithms proposed in this paper should be of interest to researches in the field of FEA and tremor suppression devices because of the feasibility verification of FEA on active tremor suppression exoskeleton. In the future, we will develop a hand exoskeleton that is driven by FEAs and conduct human tests to study the phase and frequency characteristics of finger tremor, verify the active tremor suppression ability of the proposed control methods and further improve them.

References

[1] E. Rocon, J. Belda-Lois, J. Sanchez-Lacuesta, and J. Pons, "Pathological tremor management: Modelling, compensatory technology and evaluation," *Technology and Disability*, vol. 16, no. 1, pp. 3–18, 2004.

[2] R. J. Elble, "Tremor," in *Neuro-Geriatrics: A Clinical Manual*, B. Tousi and J. Cummings, Eds. Cham: Springer International Publishing, 2017, pp. 311–326.

[3] J. Mo and R. Priefer, "Medical Devices for Tremor Suppression: Current Status and Future Directions," *Biosensors*, vol. 11, no. 4, p. 99, Apr. 2021.

[4] H. S. Nguyen and T. P. Luu, "Tremor-Suppression Orthoses for the Upper Limb: Current Developments and Future Challenges," *Frontiers in Human Neuroscience*, vol. 15, 2021.

[5] Y. Zhou, M. E. Jenkins, M. D. Naish, and A. L. Trejos, "Development of a Wearable Tremor Suppression Glove," in *2018 7th IEEE International Conference on Biomedical Robotics and Biomechatronics (Biorob)*, 2018, pp. 640–645.

[6] G. Herrnstadt and C. Menon, "Admittance-Based Voluntary-Driven Motion With Speed-Controlled Tremor Rejection," *IEEE/ASME Transactions on Mechatronics*, vol. 21, no. 4, pp. 2108–2119, 2016.

[7] G. Herrnstadt, M. J. McKeown, and C. Menon, "Controlling a motorized orthosis to follow elbow volitional movement: Tests with individuals with pathological tremor," *Journal of NeuroEngineering and Rehabilitation*, vol. 16, no. 1, p. 23, Feb. 2019.

[8] V. Skaramagkas, G. Andrikopoulos, and S. Manesis, "Towards Essential Hand Tremor Suppression via Pneumatic Artificial Muscles," *Actuators*, vol. 10, no. 9, p. 206, Sep. 2021.

[9] N. P. Fromme, M. Camenzind, R. Riener, and R. M. Rossi, "Design of a lightweight passive orthosis for tremor suppression," *Journal of NeuroEngineering and Rehabilitation*, vol. 17, no. 1, p. 47, Apr. 2020.

[10] A. Yi, A. Zahedi, Y. Wang, U.-X. Tan, and D. Zhang, "A Novel Exoskeleton System Based on Magnetorheological Fluid for Tremor Suppression of Wrist Joints," in *2019 IEEE 16th International Conference on Rehabilitation Robotics (ICORR)*, Jun. 2019, pp. 1115–1120.

[11] T. Shahid, D. Gouwanda, S. G. Nurzaman, and A. A. Gopalai, "Moving toward Soft Robotics: A Decade Review of the Design of Hand Exoskeletons," *Biomimetics*, vol. 3, no. 3, p. 17, Sep. 2018.

[12] H. Zhao, J. Jalving, R. Huang, R. Knepper, A. Ruina, and R. Shepherd, "A Helping Hand: Soft Orthosis with Integrated Optical Strain Sensors and EMG Control," *IEEE Robotics Automation Magazine*, vol. 23, no. 3, pp. 55–64, Sep. 2016.

[13] H. K. Yap, P. M. Khin, T. H. Koh, Y. Sun, X. Liang, J. H. Lim, and C.-H. Yeow, "A Fully Fabric-Based Bidirectional Soft Robotic Glove for Assistance and Rehabilitation of Hand Impaired Patients," *IEEE Robotics and Automation Letters*, vol. 2, no. 3, pp. 1383–1390, Jul. 2017.

[14] Victor Yanev, Maria Elena Giannaccini, and Sumeet S. Aphale, "Control of a Soft Actuator using a Long Short-Term Memory Neural Network," in *2022 26th International Conference on Methods and Models in Automation and Robotics (MMAR)*, 22, pp. 187–192.

[15] Wentao Sun, Nozomi Akashi, Yasuo Kuniyoshi, and Kohei Nakajima, "Physics-Informed Recurrent Neural Networks for Soft Pneumatic Actuators," *IEEE Robotics and Automation Letters*, vol. 7, no. 3, pp. 6862–6869, Jul. 2022.

[16] Y. Wang, X.-J. Liu, and H. Zhao, "Speeding up soft pneumatic actuators through pressure and flow dynamics modeling and optimization," *Extreme Mechanics Letters*, vol. 57, p. 101914, Nov. 2022.

[17] R. J. Elble, "Tremor: Clinical Features, Pathophysiology, and Treatment," *Neurologic Clinics*, vol. 27, no. 3, pp. 679–695, Aug. 2009.

[18] O. E. Dick and A. D. Nozdrachev, "Features of parkinsonian and essential tremor of the human hand," *Human Physiology*, vol. 42, no. 3, pp. 271–278, May 2016.

[19] A. Ibrahim, Y. Zhou, M. E. Jenkins, A. L. Trejos, and M. D. Naish, "Real-Time Voluntary Motion Prediction and Parkinson's Tremor Reduction Using Deep Neural Networks," *IEEE Transactions on Neural Systems and Rehabilitation Engineering*, vol. 29, pp. 1413–1423, 2021.

[20] X. Q. Shi, H. L. Heung, Z. Q. Tang, K. Y. Tong, and Z. Li, "Verification of Finger Joint Stiffness Estimation Method With Soft Robotic Actuator," *Frontiers in Bioengineering and Biotechnology*, vol. 8, 2020.

[21] K. Cho, B. van Merrienboer, C. Gulcehre, D. Bahdanau, F. Bougares, H. Schwenk, and Y. Bengio, "Learning Phrase Representations using RNN Encoder-Decoder for Statistical Machine Translation," Sep. 2014.

[22] E. Rocon, A. F. Ruiz, F. Brunetti, J. L. Pons, J. M. Belda-Lois, and J. J. Sanchez-Lacuesta, "On the use of an active wearable exoskeleton for tremor suppression via biomechanical loading," in *Proceedings 2006 IEEE International Conference on Robotics and Automation, 2006. ICRA 2006.*, May 2006, pp. 3140–3145.

IEEE Robotics and Automation Letters (RA-L) paper, presented at ICRA 2024, Yokohama, Japan. Cite as RA-L paper.